International Journal of Sciences

Research Article Volume 2 - December 2013 (12)

Artificial Neural Network Approach for Estimation of Land Surface Temperature

Maurício Roberto Veronez[1]✎, Fabiane Bordin[1], Francisco Manoel Wohnrath Tognoli[1], Anibal Gusso[1], Marcelo Kehl de Souza[1]

[1] University of Vale do Rio dos Sinos-UNISINOS, Laboratory of Remote Sensing and Digital Cartography-LASERCA, Graduate Program on Geology, AV. Unisinos, 950-CEP. 93022-000-São Leopoldo-RS, Brazil

Abstract: in this article we present an alternative method for extrapolation of Land Surface Temperature (LST) by means of Artificial Neural Networks (ANNs) based on positional variables (UTM coordinates and altitude), temperature and average air relative humidity. The study region was the Rio dos Sinos Hydrographic Basin (RSHB), Rio Grande do Sul, Brazil. For ANN training we used an NOAA-14/AVHRR satellite thermal image, with pixels size 1 x 1 km, with known information of LST on January 29, 2003. Various settings were tested in ANN training step, the one that presented the best performance was composed of only one intermediate layer (with 4 neurons and logistic sigmoid activation function). The trained network was validated with 2 simulations: in the first simulation we extrapolate the LST values of April 11, 2003 and in the second simulation we extrapolate LST values of October 15, 2003. The results of the simulations were compared with Split Window (SW) algorithm and the average discrepancies found between both models were of -0.30° C and 0.26° C, respectively, of April 11, 2003 and October 15, 2003. A strong correlation was found between both models with R^2 values exceeding 0.93 and statistically we checked that there was no difference between the LST averages values obtained by ANN and SW for 5% significance level.

Keywords: Artificial Neural Networks; NOAA Satellite Image; Land Surface Temperature; Split Window.

1. Introduction

The Land Surface Temperature (LST) constitutes a phenological parameter notably influenced by climate variations and plant water status indicator. So, its estimate is useful in monitoring work to ensure the need of crop water demand, contributing significantly in many environmental processes (Silva, 2007; Weng, Lu & Schubring, 2004).

The LST has frequently been the subject of research into scientific papers (Mallick et al., 2008; Sandholt et al., 2002; Lambin & Ehrlich, 1995; Moran et al., 1994; Gupta et al., 1997;Czajkowski & Sobrino, 2002; Becker & Li 1990; Kerr et al., 1992; Ulivieri et al., 1994; Sobrino et al., 1994) and very important for various applications in meteorology and studies of natural resources mainly in the structuring of energy balance models, biophysical and bioclimatic surface parameters (Brunsell & Gillies, 2003; Karnieli et al., 2010; Kustas & Anderson, 2009; Zhang et al., 2008) and was recognized as a high-priority parameter of the International Geosphere and Biosphere Program (IGBP) (Townshend et al., 1994).

In remote sensing, Thermal infrared (TIR) sensors can obtain quantitative information of LST and there are many available thermal infrared sensors to study LST. The Geostationary Operational Environmental Satellite (GOES) has a 4-km resolution in the termal infrared, while the NOAA-Advanced Very High Resolution Radiometer (AVHRR), Terra and Aqua-Moderate Resolution Imaging Spectroradiometer (MODIS) have 1-km spatial resolution. High resolution data from the Terra-Advanced Spaceborne Thermal Emission and Reflection Radiometer (ASTER) has a 90-m resolution and Landsat-7 Enhanced Thematic Mapper (ETM+) has a 60-m resolution in thermal region (Li, z.-l. et al., 2013).

The AVHRR is among the most used for the agro-meteorological monitoring and climate studies by enabling data acquisition in daily global scans, for having calibrated thermal spectral bands as well as wide data availability because of simultaneous operation in several meteorological satellites. From the various products that can be obtained through these data, the LST is very important due to its great usefulness in agricultural monitoring, fire detection, sea surface state monitoring, and in the studies of climate change (Gusso & Fontana, 2007; Ferreira, 2004).

Rivas (2004) advises the use of NOAA/AVHRR images adapted to the Split Windows equation (Ulivieri et al., 1994) to estimate the LST. This model relates both emissivity variable and atmospheric data.

Mauricio Roberto Veronez (Correspondence)

veronez@unisinos.br

+55-51-3591-1122 (ext. 1731)

It is a complex method because, in addition to statistical modeling hard, there is a need to work with image digital processing in the determining emissivity process.

Few studies have not used digital image processing for LST modeling. In this paper we made use of artificial intelligence techniques by means of Artificial Neural Networks to determine LST (Yang et al., 1997; Atluri et al., 1999; George, 2001; Veronez et al., 2006; Mao & Shi, 2008).

The ANNs are indicated for LST estimating because they are groupings of structured and interconnected processing units (neurons or nodes), they work analogous as neural structure of intelligent organisms (Müller & Fill, 2003). The ANNs extract the computing power of the distributed massively parallel structure and the ability to learn/generalize, enabling the resolution of complex problems (Haykin, 2001).

The ANNs works based in the human brain (Haykin, 2001) and have been successfully used in several areas of knowledge. Second Galvão et al. (1999), on the basis of non-linear structure of the ANNs is adquiring more complex features of the data, which is not always possible with the use of traditional statistical techniques.

For Müller & Fill, (2003) the great advantage of the ANNs about conventional methods is that there is no need of the knowledge of intrinsic theory problem nor the need to analyze relationships that are not fully known among the variables involved in modeling.

Despite the existence of some researches for simplify the data entry of an ANN in the process of estimating the LST, we identify that there are other options to be studied using climate data associated with thermal imaging. The objective of this study was to propose a ANN to extrapolate in time the LST values for all the Rio dos Sinos hydrographic basin/RS used as variables in modeling only altitude, position, temperature and air relative humidity. For the ANN supervised training we used LST information coming from of an NOAA thermal image rendering of January 29, 2003.

To validate the proposed model we generated two LST maps, of April 11, 2003 and October 15, 2003. The choice of these two images was because they are cloud-free and of different seasons. For these same days we also processed the NOAA satellite images and compared the discrepancies found in the values between of LST obtained by ANN and SW algorithm.

2. Artificial Neural Networks (ANN) and Resilient Backpropagation Algorithms

The ANN are groupings of processing units, called neurons or nodes, structured and interconnected, whose functionality is similar to a neural structure of intelligent organisms. The NN have a high computational power due to its parallel and distributed structure and its capacity to learn and/or make generalizations, what makes it possible to solve complex problems in a vast range of scientific knowledge(Haykin, 1999).

In view of its non-linear structure, the ANN is capable to capture the most complex characteristics from the data, which is not always possible if one uses the traditional statistical techniques or other deterministic methods. The greatest advantage of neural networks over conventional methods, such as the statistical one, is to carry out an analysis without knowledge of the intrinsic theory of the matter. Other great advantages are to analyze relations which are not fully known among the variables involved in the modelling and use a well-established technique for application by the remote sensing community (Mas & Flores, 2008).

Because of ANNs' powerful non-linear retrieval abilities, a number of attempts have been made to develop neural networks to retrieve both the surface and atmospheric biophysical variables without exact knowledge of the complex physics mechanisms (Mao et al., 2008; Aires et al., 2002b; Blackwell, 2005; Aires et al., 2002a; Wang et al., 2010).

The implementation of an ANN depends on its architecture and the training data (Mas & Flores, 2008; Schmitt et. al., 2013). It is difficult to determine the architectures and learning schemes for an ANN, which are directly related to its ability to learn and generalize. Although one or two hidden layers are recognized to be enough for most problems (Aires et al., 2002b; Mas & Flores, 2008; Sontag, 1992), a number of experiments are still required to determine what architecture-related parameters will improve the accuracy, such as the number of input and hidden nodes, the initial weight range, the activation functions, the learning rate and momentum, and the stopping criterion (Li, Z.-L. et al., 2013).

Some authors have reported the use of improved variants of backpropagation method (Heermann and Khazenie 1992, Caorsi and Gamba 1999, Gamba and Belotti 2003). Backpropagation is based on a gradient descent method (Demuth et al., 2008), which is one of many techniques of nonlinear optimization.

Other methods more efficient than gradient descente are reported in the literature. The Conjugate Gradient (Kanellopoulos and Wilkinson 1997, Idrissi et al. 2004; Del Frate et al. 2002, Del Frate et al. 2003, Del

Frate and Solimini, 2004). The Levenberg–Marquardt (Schmitt et al., 2013; Veronez et al., 2011; Chang and Islam 2000, Faure et al. 2001, Zhang et al. 2002, Combal et al. 2003, Le Maire et al. 2004, Blackwell, 2005, Muukkonen and Heiskanen 2005). A detailed description of these algorithms can be found in Haykin (1999).

We chose to use the algorithm Resilient Backpropagation (Rprop) for modeling the LST. The Rprop is an algorithm that performs batch supervised training in multilayer perceptron-like networks. This algorithm works in order to eliminate the negative influence of the partial derivative value in the weight adjustment. This influence occurs because the output value of a neuron of approximately 0 (or 1) and the expected output of 1 (or 0) imply in a derivative of approximately 0. Thus, the weight for this neuron will be minimally adjusted (Braga et al., 2007). The Rprop is capable to eliminate this problem using just the signal of the derivative, not its value. The signal indicates the direction of the weight adjustment, either increasing or decreasing the previous weight. The range of the weight adjustment is given by the "actualization value" $\Delta^{t}{}_{ji}$, as shown by Equation 1.

$$\Delta w_{ji}(t) = \begin{Bmatrix} -\Delta_{ji}(t), if \dfrac{\partial E}{\partial w_{ji}}(t) > 0 \\ +\Delta_{ji}(t), if \dfrac{\partial E}{\partial w_{ji}}(t) < 0 \\ 0, if \dfrac{\partial E}{\partial w_{ji}} = 0 \end{Bmatrix} \quad (1)$$

The Δ_{ji} is defined as an adaptation process dependent of the signal of the error derivative in relation with the weight to be adjusted, as indicated by Equation 2.

$$\Delta w_{ji}(t) = \begin{Bmatrix} \eta^{+}\Delta_{ji}(t-1), if \dfrac{\partial E(t-1)}{\partial w_{ji}}\dfrac{\partial E(t)}{\partial w_{ji}} > 0 \\ \eta^{-}\Delta_{ji}(t-1), if \dfrac{\partial E(t-1)}{\partial w_{ji}}\dfrac{\partial E(t)}{\partial w_{ji}} < 0 \\ \Delta_{ji}(t-1), if \dfrac{\partial E}{\partial w_{ji}} = 0 \end{Bmatrix} \quad (2)$$

Where:

$0 < \eta^{-} < 1 < \eta^{+}$

According with the rule of adaption used by Rprop, when the partial derivative of the error in relation to the weight w_{ji} keeps the same sign (indicating that the last adjust decreased the error), the actualization value Δ_{ji} increases by the factor η^{+} and speeds up the training convergence. When the partial derivative changes the sign (indicating that the last adjust was too much), the actualization value Δ_{ji} decreases by the factor η^{-} and changes the direction of adjustment.

3. Database and Methods

The study area was the Rio dos Sinos hydrographic basin in the State of Rio Grande do Sul as shown in Figure 1.

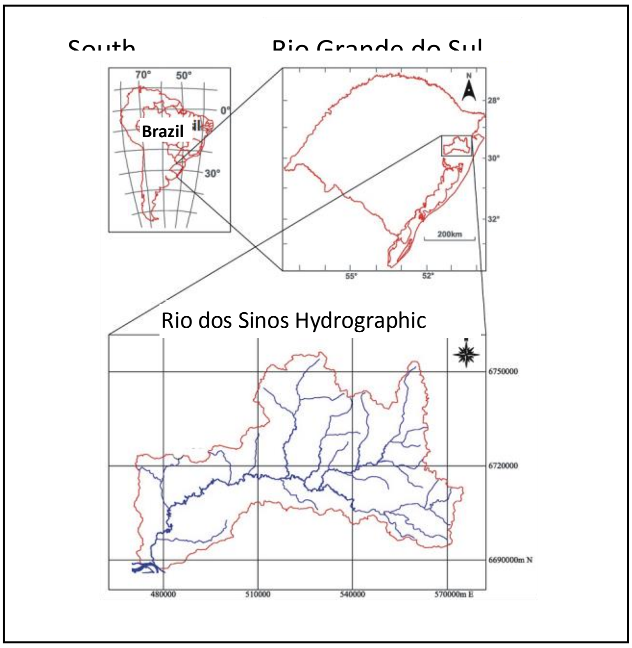

Figure 1 -location of the study area

To compose the ANN training structure we chose randomly from our database a cloud-free image from the NOAA/AVHRR satellite of January 29, 2003. To not generate systematic errors in model is important the information randomness that will compose the training database and ANN validation. (Schmitt et al.; 2013).

We corrected the image radiometrically by applying the radiance-based procedure (Kidwell, 1998). Thus, we converted the values of the Digital Numbers (DN) in Radiance (Eq. 3) and subsequently in reflectance for 1 (0.58-0.68 lm) and 2 (0.725-1.10 lm) channels and in brightness temperatures to thermal 4 (10.3-11.3 lm) and 5 (11.5-12.5 lm) channels.

$$B_{j(v)} = S_{j(v)} \cdot DN + I_{j(v)} \qquad (3)$$

Where:

- $B_{j(v)}$ corresponds to radiance (mW/sr m^2 cm^{-1});
- Sj (v) corresponds to angular coefficient calibration equation of the j channel (mW/m^2 sr cm^{-1} count);
- DN corresponds to image Digital Number;
- $I_{j(v)}$ corresponds to linear coefficient calibration equation of j channel (mW/m^2 sr cm^{-1}).

The calibration equation coefficients contain information concerning to sensor response function in a given channel. Further details about these coefficients can be found in (Kidwell, 1998).

Due to linear response lack of the AVHRR sensor, we carried out irradiances fixes (Eq. 4).

$$B_{j(v)corr} = A_j \, . \, B_{j(v)} + B_j \, . \, B_{j(v)}{}^2 + D_j \qquad (4)$$

Where:

- $B_{j\ (v)\ corr}$ corresponds to corrected radiance (mW/sr m^2 cm^{-1});
- The$_j$, B_j and D_j correspond to correction coefficients for a given j channel, due to AVHRR sensor linearity lack.

The A_j, B_j, and D_j coefficients, in the case of the NOAA-14 satellite, assume values equal to 0.92378; 0.0003822 and 3.72, respectively, for AVHRR 4 channel (Kidwell, 1998). For 5 channel these values are equal to 0.96194; 0.0001742 and 2.00, respectively. The conversion of radiance in brightness temperature for a given temperature range (265 to 320 k) is given by the equation 5:

$$T_{bj} = \frac{1{,}438833 \cdot v_j}{\ln\left(\frac{1 + 1{,}1910659x10^{-5} \cdot v_j{}^3}{B_{j(v)corr}}\right)}$$

(5)

Where:

T_{bj} corresponds to j channel brightness temperature;

νj corresponds to j channel wave number;

$B_{j\ (v)\ corr}$ corresponds to corrected radiance according to equation (4).

To estimate the Land Surface Temperature various SW algorithms (Dash et al., 2002) were developed by authors that use the AVHRR sensor information: AVHRR in NOAA-7 (price, 1984), AVHRR in NOAA-9 (Becker and Li, 1990), AVHRR in NOAA-11 (Sobrino et al., 1991), etc. The filter functions for 4 and 5 channels of the AVHRR slightly differ for each other sensor from the NOAA satellite series leading coefficients different for the SW model. This fact can lead to a considerable error in Land Surface Temperature estimation of approximately 2.3 K (Czajkowski et al., 1998).

We utilized the 4 and 5 NOAA-14/AVHRR satellite channels with the SW model coefficients (Czajkowski et al., 1998) to generate the LST image (Eq. 6) for the study area and used for ANN training. It is important take every care in the process of image calibrating. An calibration imperfect can cause an error of 0.3 K in Land Surface Temperature determining (Cooper & Asrar, 1989) and the surface emissivity variations (approximately 2%) can provide an error of 1 K (Ottle lid and Vidal-Madjar, 1992).

$$T_s = 5{,}54 + T_4 + 2{,}08 \cdot (T_4 - T_5) \qquad (6)$$

Where:

- T_s is the Land Surface Temperature;
- T_4 and T_5 match brightness temperatures of the 4 and 5 AVHRR channels, respectively, both in Kelvin.

We georeferenced the image of LST to the Universal Transverse Mercator (UTM) projection system and Hayford ellipsoid using 15 checkpoints in the ground. The root mean square error adjustment was of approximately 1 pixel. Figure 2 show the processed image with the values of LST.

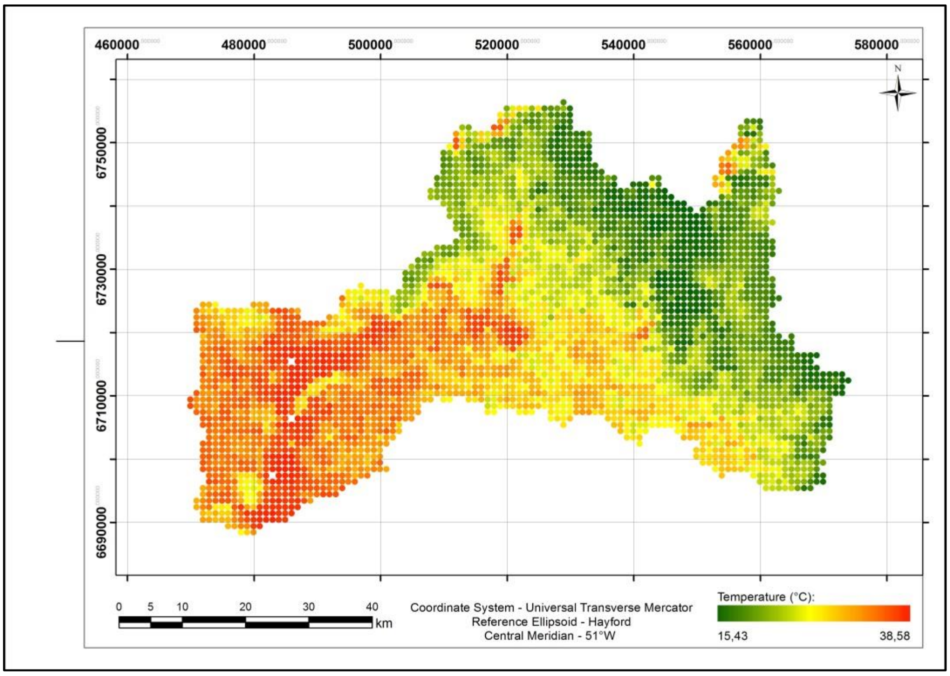

Figure 2 -NOAA image processed with Rio dos Sinos hydrographic basin LST information of January 29, 2003. Hayford ellipsoid, UTM projection and central meridian 51° W

With the processed image and georeferenced we overlay on a terrain digital model obtained from level curves with a 20 m vertical equidistance. Thus to the centroid of each pixel in the rendered image we extracted the following variables to the ANN structure: UTM coordinates (East, North, and altitude) and LST.

We used an ANN structure of type Perceptron multilayer that is based on learning by error correction. When a pattern is presented to the network for the first time, that produces an output random. The difference between this output and the desired is the error that is calculated by itself algorithm. The backpropagation algorithm firstly adjusts the weights in the output layer and then it adjusts backwards the rest of the layers to reduce the error. This process is repeated during the learning process until the error becomes acceptable (Silva *et al.*, 2004).

The neurons used in ANN were configured based on the model presented by (Haykin, 2001), as shown in Figure 3. The k index in the Synaptic weights $(w_{k,j})$ refers to the neuron in question, while the j index is associated to the synapse input signal related to weight. The weight aim is multiply the signal in the input synaptic connected to neuron. The ANNs may have additional weights, named "*bias*", and aims to avoid error generation when all the input data are null, because the weights array not suffer training changes. The activation function is of internal order. The neuron takes a decision about what to do with the sum resulting value of the weighted inputs. The transfer function is an output function or logical threshold. It controls the activation intensity to obtain the desired network performance.

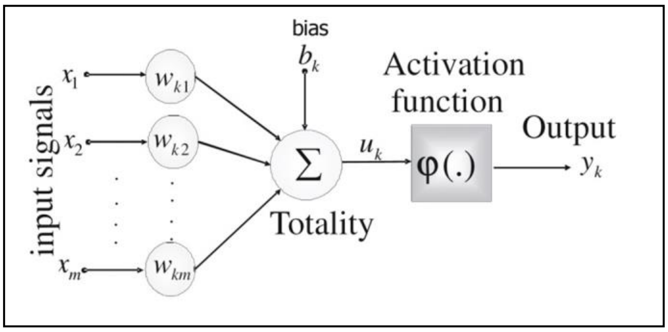

Figure 3 – The artificial neurons structure used in ANN. Adapted from Haykin (2001).

The Figure 3 can be mathematically expressed in equations 7, 8 and 9.

$$u_k = \sum_{j=1}^{n} \left(w_{k,j} \cdot x_j \right) \qquad (7)$$

$$\upsilon_k = u_k + b_k \qquad (8)$$

$$y_k = \varphi(\upsilon_k) \qquad (9)$$

Where:

- u_k is the linear combiner output (additive junction);
- $w_{k,j}$ *are the* synaptic weights;
- x_j are the input variables;
- υ_k is the activation potential;
- *b* is the *bias*;
- y_k is the k neuron output signal;
- $\varphi(\upsilon_k)$ is the activation function.

We used a network supervised training with the Resilient Backpropagation (Rprop) algorithm, shown in item 2. In this case we trained the ANN in inputs and outputs pairs, i.e., for each input supplied to the network there is an expected output which is also provided for the training. The network produces an output answer that is compared with the desired output (that was provided). The difference between the network response and the answer desired (known) generates a residue (error). This error is used to calculate the necessary adjustment to the network synaptic weights, that will be corrected until the network response matches the output desired. This is the process of error minimization (Haykin, 2001). The equation 10 shows the MSE (Mean Squared Error) function to be minimized that we used in training phase (Haykin, 2001):

$$MSE = \frac{\sum_{j=1}^{n} (d_j - y_j)^2}{n} \qquad (10)$$

Where:

- d_j *is the* ANN desired output value;
- y_j *is the* obtained output value;

The input and output variables that we used were:
Input variables: UTM (E); UTM (N); orthometric altitude; air average Temperature; air average humidity.

Output variable: LST

We carried out tests to select an ANN that provides the best performance to LST estimate, modifying the number of intermediate layers, the per layer neurons numbers and the activation function.
An activation function, φ(v), defines the output of a neuron in terms of the linear combination of inputs, v. There are different kinds of activation functions: the threshold function, the piecewise-linear function, and the logistic (sigmoid) function (Mas & Flores, 2008). We use logistic activation function (Mas & Flores, 2008) defined by equation (11).

$$\varphi(v_k) = \frac{1}{1 + e^{-av}} \qquad (11)$$

We trained the ANN with information from a thermal image processing of the NOAA satellite of January 29, 2003. The generated image have 1 x 1 km pixel size, and amounted 3737 points in the training process. The temperature and the average relative humidity were obtained, in this date, of the existing weather stations on the RSHB.

With the ANN trained we generated 2 LST RSHB images of April 11, 2003 and October 15, 2003. We also generated, for the 2 dates, 2 images from the SW algorithm, and analyzed statistically the LST values obtained for ANN and SW. We used, in the results analysis, the statistical test "t-Student" and R^2 coefficient determination of the linear regression between the LST values of ANN and SW.

3. Results and Discussion

The ANN best performance has an input layer (5 variables), an intermediate layer (with 4 neurons) and an output layer (with 1 neuron) as shown in Figure 4. The fact that we found a network structure with only a intermediate layer is agreeing to the results found by Kumar et al. (2002) and Zanetti et al. (2008). These authors modeled the evapotranspiration and concluded that an ANN with only a intermediate layer was enough to represent the non-linear relationship between the climatic elements and the modeled variable.

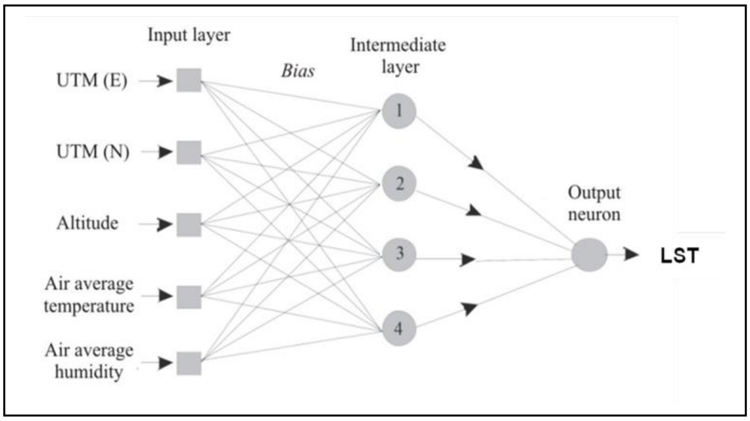

Figure 4 – The neural network structure used in the modeling of LST

The activation function that we used was the sigmoidal logistic and the number of training cycles was 600.

Figures 5(A) and 5(B) shows LST maps generated by ANN and SW models, respectively, on April 11, 2003.

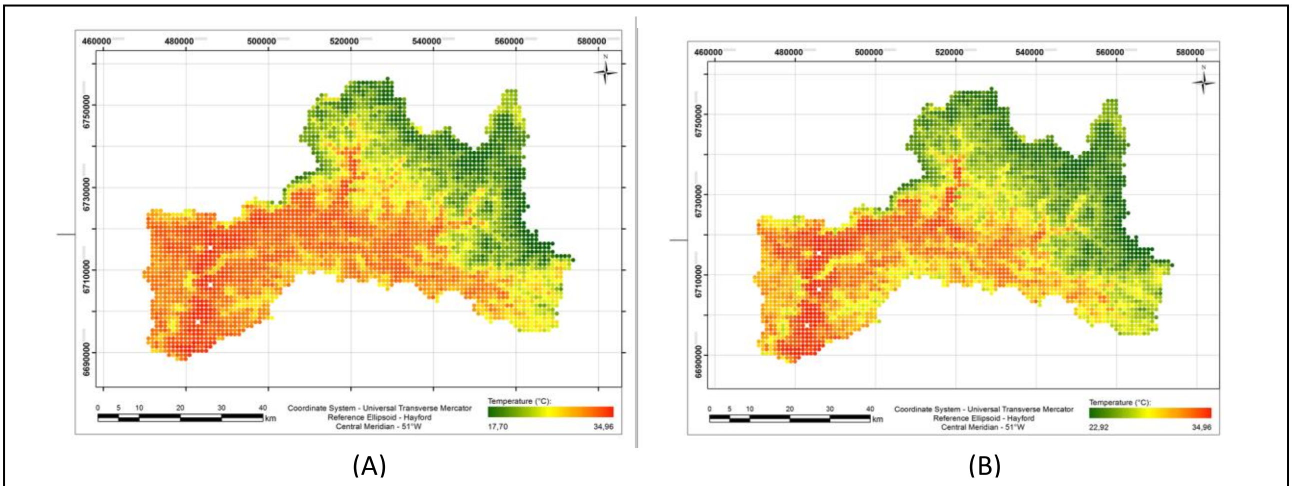

Figure 5 - LST maps generated by ANN (A) and LST maps generated by SW (B)

We found that both maps are similar, with discrepancies average, minimum and maximum of LST between the models of -0.30°C -1.23°C and 3.08°C, respectively (figure 6). This shows that the proposed neural model generated a compatible pattern with the SW algorithm.

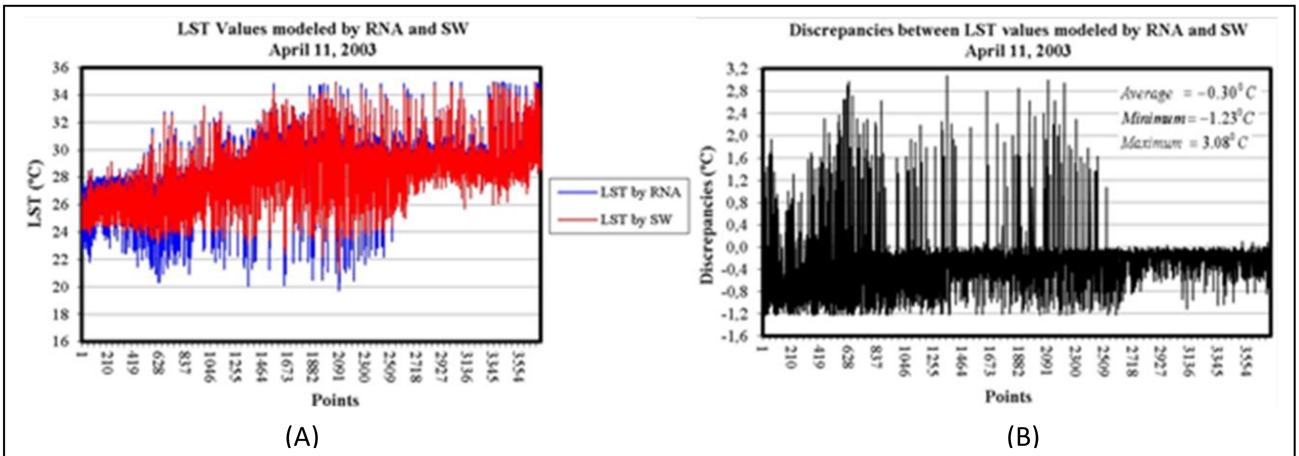

Figure 6 - LST values modeled by RNA and SW of April 11, 2003 (A) and discrepancies between LST values

modeled by RNA and SW of April 11, 2003 (B).

Figura 7a – Discrepâncias absolutas entre valores de TS modelados por RNA e SW referentes ao período 11/04/2003.

Figura 7b – **V**alores de TS modelados por RNA e SW referentes ao período 11/04/2003.

The largest discrepancies between the LST values processed with ANN and SW, are concentrated at temperatures below 23°C (Figure 6A). This can be associate to the network input variables (temperature and air average humidity), that not may be representative for the whole hydrographic basin, because we have established the average values based on meteorological stations located within the study area. We cannot also rule out that these large discrepancies are associated with SW model that provides a 1.5°C average error to LST (Coll & Caselles, 1997).

In summary, both models are closely correlated to most of the hydrographic basin, according the R^2 = 0.9406 linear regression analysis (Figure 7).

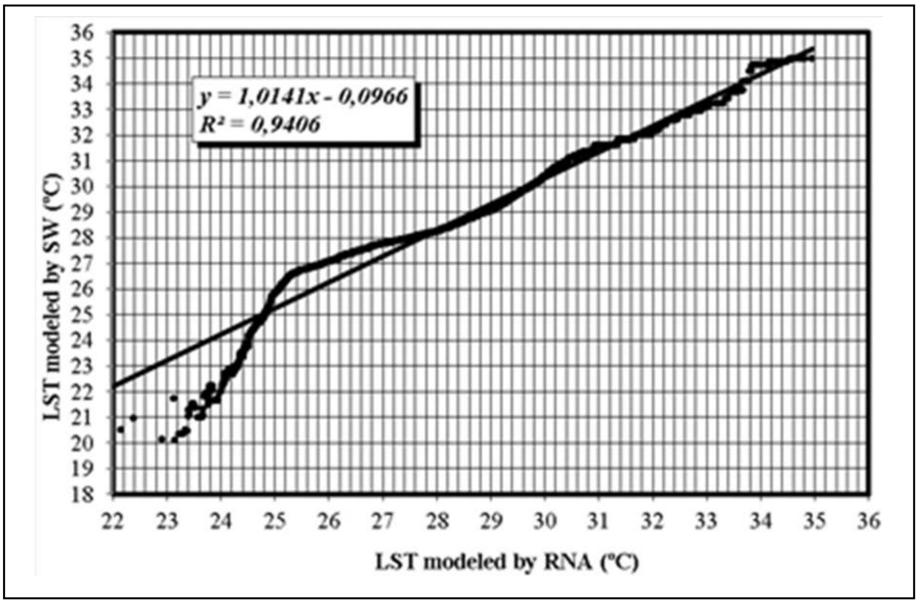

Figure 7 – Linear regression between LST values modeled by ANN and SW of April 11, 2003.

In Figure 8 are shown the LST values modeled by ANN and SW algorithm, respectively, of October 15, 2003.

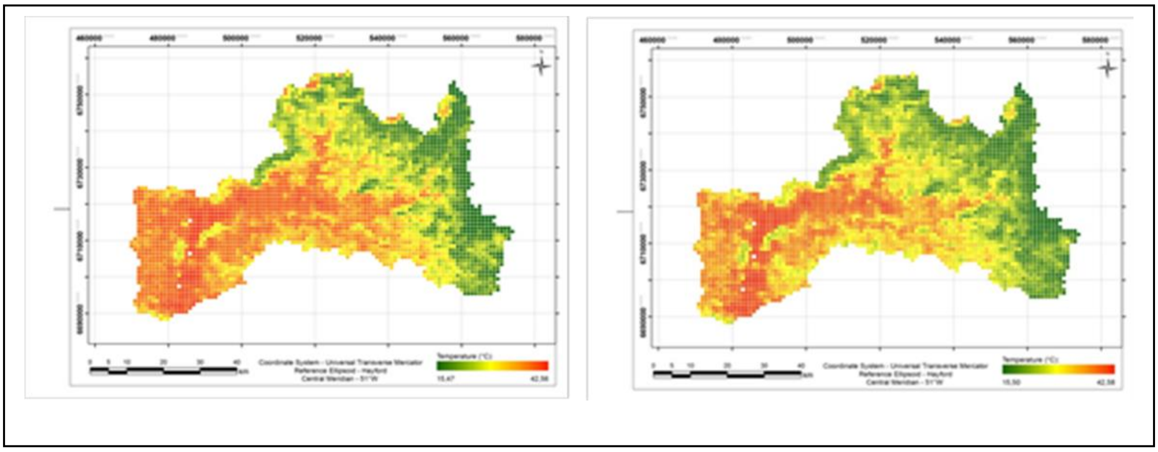

(A) (B)

Figure 8 - LST values modeled by RNA and SW of October 15, 2003 (A) and discrepancies between LST values modeled by RNA and SW of October 15, 2003 (B).

Figura 7a – Discrepâncias absolutas entre valores de TS modelados por RNA e SW referentes ao período 11/04/2003.

Figura 7b – **V**alores de TS modelados por RNA e SW referentes ao período 11/04/2003.

We found that both maps (Figure 11a and 11b) are similar with discrepancies of average, minimum and maximum of LST values between the both models: -0.26°C, -1.00° C and 3.07° C, respectively. This shows that the proposed neural model also generated a pattern compatible with the SW algorithm in this date.

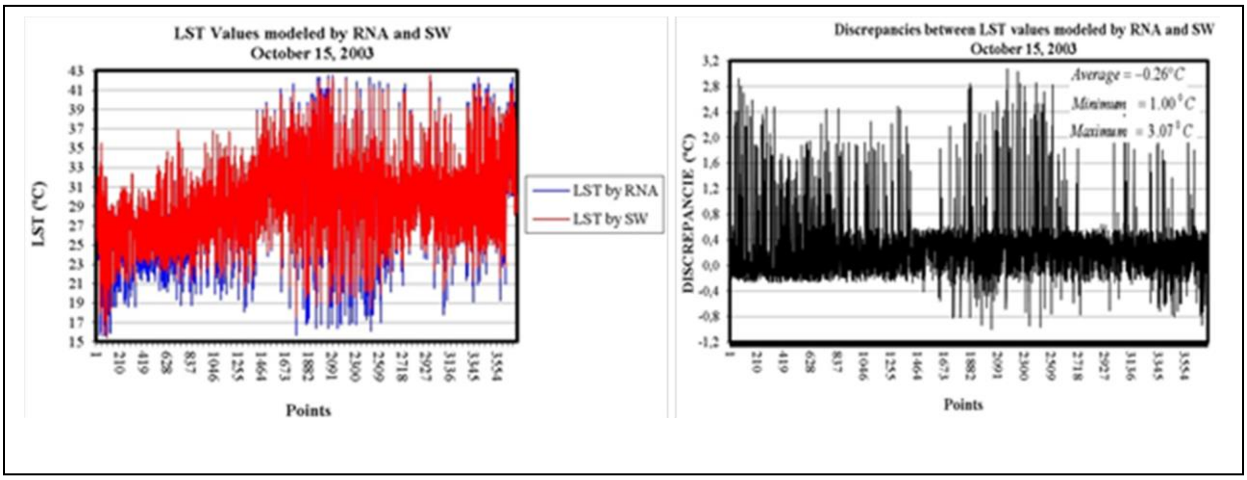

(A)

(B)

Figure 8 - LST values modeled by RNA and SW of October 15, 2003 (A) and discrepancies between LST values modeled by RNA and SW of October 15, 2003 (B).

We perceived a subtle improvement (Figure 11b) in the fit between ANN and SW models compared with April 11, 2003. The discrepancy values are compatible in both simulations with few values above 2.8 º C and most of points between -0.8 and 0.8° C.

In regression analysis (Figure 9) we also found a strong correlation between the LST values modeled by ANN and SW (R^2 = 0.9871).

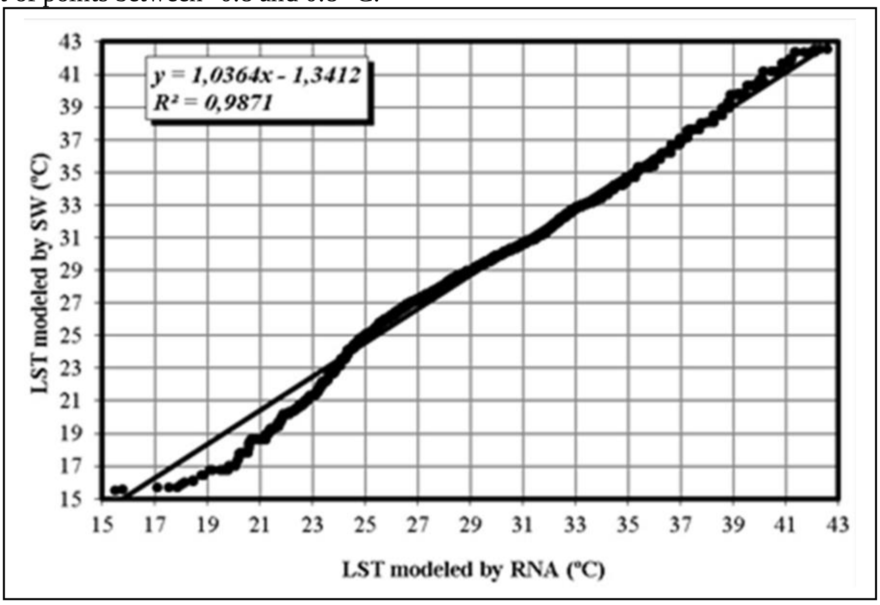

Figure 9 – Linear Regression between LST values modeled by ANN and SW of October 15, 2003.

For the two experiments concerning to the days April 11 and October 15, we applied the hypothesis test (Student's t) and found that the ANN model were able to process LST values with equal values to the SW average values, for significance level of 5%.

4. Conclusions

We proposed a simple method to determine LST values based on ANN with controlled training through an NOAA thermal imaging of January 29, 2003. The variables involved in the model were positional information (UTM coordinates and altitude) and climatic (temperature and air relative humidity).

The experiments we conducted on Rio dos Sinos hydrographic basin- Brazil, in April 11, 2003 and October 15, 2003 showed statistically that, for LST values, the modeling ANN did not differ from of the SW algorithm to a of 5% significance level. We also found a strong correlation between the LST values obtained by ANN and SW, with R^2 values equal to 0.9375 and 0.9871, respectively, of April 11, 2003 and October 15, 2003. To simulation of April 11, 2003 the largest discrepancies in the LST values were concentrated in the temperatures below 23ºC and this is due to the network input variables (temperature and air average humidity). This may not be representative for all hydrographic basin because they are average values obtained in some weather stations located within of the study area.

The great advantage provided by ANN modeling was the simplicity in generating maps of LST, it is a method based on variables of easy access, which does not occur with the SW model, even though in some temperature ranges the discrepancies between both models are greater than 1.8° C.

Finally, we think that is important to perform new experiments to better the effectiveness of the proposed method by testing in other seasons and with field confirmation of LST values with laser sensors.

References

1) Aires, F., Chédin, A., Scott, N. A., & Rossow, W. B. (2002). A regularized neural net approach for retrieval of atmospheric and surface temperatures with the IASI instrument. Journal of Applied Meteorology, 41, 144–159.
2) Aires, F., Rossow, W. B., Scott, N. A., & Chédin, A. (2002). Remote sensing from the infrared atmospheric sounding interferometer instrument, 2, Simultaneous retrieval of temperature, water vapor, and ozone atmospheric profiles. Journal of Geophysical Research, 107, 4620.
3) Atluri, V.; Hung, C. C.; Coleman, T. L. Artificial Neural Network for Classifyng and Predicting Soil Moisture and Temperature Using Levenberg-Marquardt Algorithm. Alabama, p. 10-13, 1999.
4) Becker, F., Li, Z.-L. Temperature-independent spectral indices in thermal infrared bands. Remote Sensing of Environment, v. 32, n. 1, p. 17–33, 1990.
5) BLACKWELL, W.J., 2005, A neural-network technique for the retrieval of atmospheric temperature and moisture profiles from high spectral resolution sounding data. IEEE Transactions on Geoscience and Remote Sensing, 43, pp. 2535–2546.
6) Braga, A. P., Carvalho, A. P. L. F., & Ludermir, T. B. (2007). Redes neurais artificiais: teorias e aplicações (2nd ed.). Rio de Janeiro: LTC.
7) Brunsell, N. A., & Gillies, R. R. (2003). Length scale analysis of surface energy fluxes derived from remote sensing. Journal of Hydrometeorology, 4, 1212–1219.
8) Coll, C., Caselles, V. A split window algorithm for land surface temperature from advanced very high resolution radiometer data: Validation and algorithm comparison. Journal of Geophysical Research, v. 102, n. 14, p. 16697-16713, 1997.
9) COMBAL, B., BARET, F., WEISS, M., TRUBUIL, A., MACe, D., PRAGNERE, A., MYNENI, R., KNYAZIKHIN, Y. and WANG, L., 2003, Retrieval of canopy biophysical variables from bidirectional reflectance using prior information to solve the ill-posed inverse problem. Remote Sensing of Environment, 84, pp. 1–15.
10) Cooper, D. I., Asrar, G. Evaluating atmospheric correction models for retrieving surface temperatures from the AVHRR over a tallgrass prairie*1. Remote Sensing of Environment, v. 27, n. 1, p. 93–102, 1989
11) Czajkowski, K.P., Goward, S.N., Ouaidrari, H. Impact of AVHRR filter functions on surface temperature estimation from the split window approach. International Journal of Remote Sensing, v. 19, n. 10, p. 2007–2012, 1998.
12) Czajkowski, K. P.; Sobrino, J. A.; Vermote, E. Land surface temperature estimation from AVHRR thermal infrared measurements: An assessment for the AVHRR Land Pathfinder II data set. Remote Sensing of Environment, v.81, n. 1, p. 114-128, 2002.
13) Dash, P., Gottsche, F.M., Olesen, F.S., Fischer, H. Land surface temperature and emissivity estimation from passive sensor data: theory and practice-current trends. International Journal of Remote Sensing, v. 23, n. 13, p. 2563–2594, 2002.
14) Del Frate, F. Solimini, D. (2004). On neural network algorithms for retrieving forest biomass from SAR data, IEEE Transactions on Geoscience and Remote Sensing, 42 (1),24-34
15) Dousset, B. & Gourmelon, F., 2003. Satellite multi-sensor data analysis of urban surface temperatures and landcover, ISPRS Journal of Photogrammetry and Remote Sensing. 58, (1-2), 43-54.
16) Esquerdo, J. C. D. M.; Antunes, J. F. G.; Baldwin, D. G.; Emery, W. J.; Zullo Jr, J. An automatic system for AVHRR land surface product generation. International Journal of Remote Sensing, v.27, n.18, p.3925-3942, 2006.
17) Ferreira, N.J. (Coordenador) Aplicações ambientais brasileiras dos satélites NOAA e TIROS-N. São Paulo: Oficina de Textos, 2004
18) Galvão, C. O.; Valença, M. J. S.; Vieira, V. P. P. B.; Diniz, L. S.; Lacerda, E. G. M.; Carvalho, A. C. P. L. F; Ludermir, T. B. Sistemas inteligentes: Aplicações a recursos hídricos e ciências ambientais. Porto Alegre: UFRGS/ABRH, 1999, 246p.
19) George, R. K. Prediction of soil temperature by using artificial neural networks algorithms. Nonlinear Analysis, v. 47, n. 3, p. 1737-1748, 2001.
20) Gupta, R.K.; Prasad, S.; Sesha-Sai, M.V.R.; Viswanadham, T.S. (1997) The estimation of surface temperature over an agricultural area in the state of Haryana and Panjab, India, and its relationship with the Normalized Difference Vegetation Index (NDVI), using NOAA-AVHRR data. International Journal of Remote Sensing, 18: 3729-3741.
21) Gusso, A.; Fontana, D. C.; Gonçalves, G. A. (2007) Mapeamento da temperatura da superfície terrestre com uso do sensor NOAA/AVHRR. Pesquisa Agropecuária Brasileira. Brasília, 42: 231-237.
22) Haykin, S. Redes Neurais: princípios e prática. Porto Alegre: Editora Bookman, 2001, 900p.
23) Karnieli, A., Agam, N., Pinker, R. T., Anderson, M., Imhoff, M. L., & Gutman, G. G. (2010). Use of NDVI and land

surface temperature for drought assessment: Merits and limitations. Journal of Climate, 23, 618–633.
24) Kerr, Y. H., Lagouarde, J. P., & Imbernon, J. (1992). Accurate land surface temperature retrieval from AVHRR data with use of an improved split window algorithm. Remote Sensing of Environment, 41, 197–209.
25) Haykin, S. (1999). Neural networks: a comprehensive foundation (2nd ed.). New Jersey: Prentice-Hall.
26) Kustas, W., & Anderson, M. (2009). Advances in thermal infrared remote sensing for land surface modeling. Agricultural and Forest Meteorology, 149, 2071–2081.
27) Kidwell, K. B. NOAA Polar Orbiter Data Users Guide. NOAA, US Department of commerce, Washington DC, 1998
28) Kumar, M.; Raghuwanshi, N. S.; Singh, R.; Wallender, W. W.; Pruitt, W. O. Estimating evapotranspiration using artificial neural network. Journal of Irrigation and Drainage Engineering, v. 128, n. 4, p.224-233, 2002.
29) Lambin E.F. and Ehrlich D., 1995. Combining vegetation indices and surface temperature for landcover mapping at broad spatial scales, International Journal of Remote Sensing, 16(3), pp.573-579.
30) Le Maire, G., Fran, C. and Dufrene, E., 2004, Towards universal broad leaf chlorophyll indices using PROSPECT simulated database and hyperspectral reflectance measurements. Remote Sensing of Environment, 89, pp. 1–28.
31) Li, Z.-L., Tang, B-H., Wu, H., Ren, H., Yan, G., Wan, Z., Trigo, I. F., Sobrino, J. A. (2013). Satellite-derived land surface temperature: Current status and perspectives. Remote Sensing of Environment 131, 14–37.
32) Mallick , J., Kant, Y., Bharath, B.D. Estimation of land surface temperature over Delhi using Landsat-7 ETM+, J. Ind. Geophys. Union, 12(3), 131-140
33) Mao, K; Shi, J. A Neural Network Technique for Separating Land Surface Emissivity and Temperature From ASTER Imagery. IEEE Transactions on Geoscience and Remote Sensing, v. 46, n. 1, p. 200-208, 2008.
34) Mas, J. F., & Flores, J. J. (2008). The application of artificial neural networks to the analysis of remotely sensed data. International Journal of Remote Sensing, 29, 617–663.
35) Moran, M. S.; Clarke, T. R.; Inoue, Y.; Vidal, A. (1994) Estimating crop water deficit using the relation between surface-air temperature and spectral vegetation index. Remote Sensing of Environment, 49: 246– 263.
36) Muller, M.; Fill, H. D. Redes Neurais aplicadas na propagação de vazões. In: Simpósio Brasileiro de Recursos Hídricos, 15, Curitiba. Anais..., Curitiba: ABRH, 2003. Artigos, p. 1-15. CD-ROM, On-line. Disponível em: < http://www.lactec.org.br/OInstituto/downloads/Biblioteca/2003/065_2003.pdf>. Acesso em: 11 set. 2008.
37) Muukkonen, P. and Heiskanen, J., 2005, Estimating biomass for boreal forests using ASTER satellite data combined with standwise forest inventory data. Remote Sensing of Environment, 99, pp. 434–447.
38) Ottle, C., Vidal-Madjar, D. Estimation of land surface temperature with NOAA 9 data. Remote Sensing of the Environment, v. 40, n. 1, p. 27–41, 1992.
39) Price, J. C. Land surface temperature measurements from the split window channels of the NOAA 7 advanced very high resolution radiometer. Journal of Geophysical Research, v. 89, n. 5, p. 7231–7237, 1984.
40) Rivas, R. E. Propuesta de un modelo operativo para la estimación de la evapotranspiración. 2004. 140 p. Tesi Doctoral - Universitat de València, València, Spain. 2003.
41) Schmitt, P., Veronez, M. R., Tognoli, F. M. W., Todt, V., Lopes, R. C., Da Silva, C. A. U. (2013). Electrofacies Modelling and Lithological Classification of Coals and Mud-bearing Fine-grained Siliciclastic Rocks Based on Neural Networks. Earth Science Research; V. 2, n.1, n. 1, 193-208.
42) Silva, J. W. F. 2007: Estimativa da temperatura da superfície do solo de uma região semi-árida a partir do IRMSS (banda 4) do CBERS-2. In: Simpósio Brasileiro de Sensoriamento Remoto (SBSR), 13., 2007, Florianópolis. Anais... São José dos Campos: INPE, 2007. Artigos, p. 1159-1166. CD-ROM, On-line. ISBN 978-85-17-00031-7. Disponível em: < http://marte.dpi.inpe.br/col/dpi.inpe.br/sbsr@80/2006/11.16.01.21/doc/1159-1166.pdf>. Acesso em: 07 ago. 2008.
43) Silva, A. N.; Ramos, R.; Souza, L.; Rodrigues, D.; Mendes, J. SIG – Uma plataforma para introdução de técnicas emergentes no planejamento urbano regional e de transportes. São Carlos: Editora da EESC/USP, 2004, 221p.
44) Sobrino, J., Coll, C., Caselles, V. (1991) Atmospheric correction for land surface temperature using NOAA-11 AVHRR channels 4 and 5. Remote Sensing of Environment, v. 38, n. 1, p. 19–34.
45) Sobrino, J. A., Li, Z.-L., Stoll, M. P., & Becker, F. (1994). Improvements in the split-window technique for land surface temperature determination. IEEE Transaction on Geosciences and Remote Sensing, 32, 243–253.
46) Sandholt, L.; Rasmunssen, K.; Andersen, J. (2002) A simple interpretation of the surface temperature/vegetation index space for assessment of surface moisture status. Remote Sensing of Environment, 79: 213-224.
47) Sontag, E. D. (1992). Feedback stabilization using two-hidden-layer nets. IEEE Transactions on Neural Networks, 3, 981–990.
48) Townshend, J. R. G., Justice, C. O., Skole, D., Malingreau, J. P., Cihlar, J., Teillet, P., et al. (1994). The 1 km resolution global data set: needs of the International Geosphere Biosphere Programme. International Journal of Remote Sensing, 15, 3417–3441.
49) Ulivieri, C.; Castronuovo, M. M.; Francioni, R.; Cardilo, A. A split window algorithm for estimating land surface temperature from satellites. Advances in Space Research, v.14, n.3, p.59-65, 1994
50) Veronez, M. R.; Thum, A. B.; Luz, A. S.; Da Silva, D. R. 2006. Artificial Neural Network applied in the determination of Soil Surface Temperature-SST. In: International Simposium Accuracy Assessment in Natural Resources and Environmental Sciences, (Accuracy 2006), 7., Lisboa-Portugal. Anais... Lisboa, IGP, 2006. Artigos, p. 889-898. Impresso. ISBN 972-886-727-I
51) Veronez, M. R., De Souza, S. F.; Matsuoka, M. T., Reinhardt, A. O., Da Silva, R. M. (2011), Regional Mapping of the Geoid Using GNSS (GPS) Measurements and an Artificial Neural Network. Remote Sensing, 3, 668-683.
52) Yang, C. C.; Prassher S. O.; Mehuys G. R.; Patni, N. K. Application of artificial neural networks for simulation of soil temperature. Transactions of the ASAE, v. 40, n. 3, p. 649-656, 1997.
53) Wang, N., Tang, B. H., Li, C., & Li, Z.-L. (2010). A generalized neural network for simultaneous retrieval of atmospheric profiles and surface temperature from hyperspectral thermal infrared data. IEEE International Geoscience and Remote Sensing Symposium (pp. 1055–1058). Honolulu, USA: IEEE.
54) Weng, Q., Lu, D. & Schubring, J., 2004. Estimation of land surface temperature-vegetation abundance relationship for urban heat island studies, Remote Sensing of Environment, 89(4), 467-483.
55) Zanetti, S. S.; Sousa, E. F.; De Carvalho, D. F.; Bernardo, S. Estimação da evapotranspiração de referência no Estado do Rio de Janeiro usando redes neurais artificiais. Revista Brasileira de Engenharia Agrícola e Ambiental, v. 12, n.2, p.174-180, 2008.
56) Zhang, R., Tian, J., Su, H., Sun, X., Chen, S., & Xia, J. (2008). Two improvements of an operational two-layer model for terrestrial surface heat flux retrieval. Sensors, 8, 6165–6187.
57) Zhang, y., Pulliainen, J., Koponen, s. and Hallikainen, m., 2002, Application of na empirical neural network to surface water quality estimation in the Gulf of Finland using combined optical data and microwave data. Remote Sensing of Environment, 81, pp. 327–336.